NASA
Technical
Paper
2756

September 1987

Effects of Aerosols and Surface Shadowing on Bidirectional Reflectance Measurements of Deserts

David E. Bowker
and Richard E. Davis

NASA

NASA Technical Paper 2756

1987

Effects of Aerosols and Surface Shadowing on Bidirectional Reflectance Measurements of Deserts

David E. Bowker
and Richard E. Davis

Langley Research Center
Hampton, Virginia

National Aeronautics
and Space Administration

Scientific and Technical Information Office

Introduction

Desert surfaces are probably one of the most stable of the Earth's natural targets for remote sensing measurements. When viewed from space these surfaces can, in effect, represent the solar diffuser plates or thermal blackbodies generally needed for in-flight instrument calibration. As an example, the bright gypsum sands and the nearby dark lava flows at the White Sands National Monument, New Mexico, are occasionally used as relative comparison targets for satellite sensors. Staylor (1986) has discussed the selection and directional models of several deserts to be used as validation targets for three Earth Radiation Budget Experiment (ERBE) missions. These targets will serve as independent calibration sources in the event that the onboard calibration systems degrade or do not function as designed.

The bidirectional reflectance properties of one of these deserts, the Saudi Arabian desert, was investigated by J. M. Davis (1982) during the Summer Monsoon Experiment (Summer Monex) by using high-altitude aircraft at a time of large solar zenith angles. A comparison of the bidirectional reflectance determined from his data with that of Salomonson (1968) for low-altitude measurements of the White Sands desert showed significant differences between the two plots. (Davis reported an rms difference of 0.43.) The expectation was that the shape of the bidirectional reflectance curves should have been similar, even considering the differences in reflectances of deserts. Davis attributed these discrepancies to the forward scattering of the dust-laden atmosphere prevalent during Summer Monex. The three optical parameters related to the aerosol concentration and needed to compute the atmospheric effects are optical depth, single-scattering albedo, and scattering phase function. The relative importance of aerosol scattering and absorption in remote sensing has been discussed by Fraser and Kaufman (1983), and the effects of surface reflectances on the radiation emerging from the top of the atmosphere have been presented by Fitch (1981). A study of the reflectance measurement errors produced by uncertainties in the input model parameters has been made by Bowker et al. (1983).

The present paper is concerned with (1) a modeling of the influence of atmospheric aerosols on the remote sensing of bidirectional reflectances of desert targets, (2) a modeling of the effects of surface shadowing, and (3) a comparison of the results of these models with the flight results of Davis. This study was done only for large solar zenith angles because the effects of aerosols and shadows are more pronounced at these angles and, more importantly, Davis' data were obtained for solar zenith angles of 70° to 80°. Although it is possible to approximate Davis' results, it is felt that a surface reflectance model with a smaller specular component would have permitted using a more realistic set of atmospheric parameters in the simulations.

Symbols

B	Volz turbidity parameter
E(dir)	direct component of surface irradiance, W-m^{-2}
E(tot)	sum of direct and diffuse components of surface irradiance, W-m^{-2}
$F(B)$	cumulative frequency of daily average turbidity for one of three representative distributions, percent
f/b	forward/backward scattering ratio
H/λ	ratio of height of repetitive surface feature to wavelength
h	altitude, km
L(indir)	surface radiance resulting from diffuse irradiance component, W-m^{-2}-sr^{-1}
L(path)	path radiance between surface and sensor, W-m^{-2}-sr^{-1}
L(tot)	surface radiance resulting from direct and diffuse irradiance components, W-m^{-2}-sr^{-1}
n	complex index of refraction
n_{re}	real component of index of refraction
n_{im}	imaginary component of index of refraction
$P(\theta)$	phase function
T	atmospheric transmission from surface to sensor
V	meteorological visibility, km
VR	visual range, km
λ	wavelength, μm
θ	scattering angle, deg
θ_r	sensor zenith angle, deg
θ_s	solar zenith angle, deg
ρ	surface reflectance at nadir
ρ_b	surface background reflectance
τ	optical depth
ψ	azimuth angle (relative to Sun direction), deg

ω_o	single-scattering albedo

Abbreviations:

AFGL	Air Force Geophysics Laboratory
BRF	bidirectional reflectance factor
ERBE	Earth Radiation Budget Experiment
ERIM	Environmental Research Institute of Michigan
Monex	Monsoon Experiment
Norm. refl.	normalized reflectance
rms	root mean square

Desert Reflectance Model

The spectral reflectance of a collection of representative desert surfaces can be found in a report by Bowker et al. (1985). Most of these data were obtained with nadir looking, narrow-field-of-view sensors during small solar zenith angles. Ashburn and Weldon (1956) measured the reflectance of desert surfaces by using a sensor with a 2π steradian field of view; when these measurements are normalized by the total radiation incident on the surface, the results are referred to as albedo, an important term in climatological studies. Surface reflectances in the visible region of the spectrum varied from less than 0.1 for dark basalt to greater than 0.7 for salt beds. In this investigation, then, reflectances of 0.1, 0.4, and 0.7 will be taken to represent the average and typical range of values for desert environments.

The reflections from most natural surfaces are anisotropic, particularly at large solar zenith angles. Kimes et al. (1985) have measured the bidirectional reflectance factors for several natural surfaces of Northern Africa, ranging from plowed fields to salt plains. Salomonson (1968) determined the reflectance of a dry desert lake bed in California and the white gypsum sands near Alamogordo, New Mexico. The white sands were the most isotropic of the surfaces he studied. The normalized reflectances, i.e., the ratio of reflectance at the sensor zenith angle θ_r to the reflectance at nadir, of three desert surfaces from Salomonson (1968) and Kimes et al. (1985) are shown in figure 1 for the principal plane. (The fundamental viewing geometry for this investigation is illustrated in figure 2, where the principal plane, defined as being normal to the surface and passing through the Sun and the origin of the reference system, is shown.) Note that the minimum reflectance of the white sands is located near nadir; these curves will be discussed in more detail later. The normalized bidirectional reflectance factor (BRF) of the white sands, for a solar zenith angle of 76° to 82°, is shown in figure 3; this is also referred to as an anisotropic reflectance diagram. Since Davis used Salomonson's data in his paper, these data will be used here as an input in the radiative transfer calculations. For those interested in albedo, a technique for inferring the albedo of the Earth's surface from multiple off-nadir view angles has been presented by Kimes and Sellers (1985).

Two factors contributing to anisotropy in surface reflectance are surface roughness and shadowing. The importance of shadowing in bidirectional reflectances has recently been studied by Cooper and Smith (1985) and Norman et al. (1985). Both Salomonson (1968) and Kimes et al. (1985) attributed the minimum reflectance in the extreme forward-scattering direction of rough surfaces, such as soils and plowed fields, to shadowing. Insofar as the bidirectional data (fig. 3) selected for the present study appear to be relatively free of such effects, an independent model for shadowing is incorporated in the event that the surface includes such features as coarse regolith, dunes, and hills. Figure 4 illustrates the geometry of the surface roughness model in the principal plane where a terrain feature of height H has a periodic occurrence with horizontal wavelength λ. The ratio H/λ determines the percent of surface shadowing for a given solar zenith angle. The nominal value of $H/\lambda = 0.134$ used in this study gives a sunlight/shadow ratio of 1 at nadir for a solar zenith angle of 75°. For measurements out of the principal plane, shadowing is dependent on $\cos(\psi)$.

Radiative Transfer Program

Radiative transfer determinations were made with two existing computer programs. A version of the ERIM radiative transfer model developed by Turner (1974) was used to account for single- and multiple-scattering effects in Rayleigh scattering and aerosol scattering as well as to account for ozone absorption over a wavelength range of 0.27 to 2.20 μm. The AFGL LOWTRAN 5 radiative transfer model, described by Kneizys et al. (1980), accounted for zero-order scattering and gaseous absorption effects over a wavelength range of 0.25 to 28.5 μm. The spectral interval of interest for this investigation was limited to 0.55 to 0.85 μm; all the data presented here are for the representative central wavelength of 0.7 μm.

In our version of the ERIM program, the target reflectance ρ is surrounded by a uniform background reflectance ρ_b. The two reflectances are made equal in this study. The solar zenith angle θ_s was nominally set at 75° to agree with Davis' measurements, whereas the sensor nadir angle θ_r and the relative azimuth angle ψ were varied at regular intervals.

Because of the assumed hemispheric symmetry of the bidirectional reflectance about the principal plane, the relative azimuth angle range simulated was limited to 0°to 180°. The altitude h was set at 10 km to agree with the altitude of Davis' measurements.

The molecular effects (Rayleigh scattering) can be easily accounted for with a standard atmosphere, but the aerosol effects are variable and require the atmospheric conditions to be specified for each calculation. Three optical parameters are needed for simulation of the atmospheric effects: they are the optical depth τ, which determines the extinction of light; the single-scattering albedo ω_o, which is that fraction of attenuation due to scattering; and the scattering phase function $P(\theta)$, which gives the probability of scattering in a particular direction.

Four values for the single-scattering albedo were investigated: 0.96, 0.81, 0.65, and 0.50. The 0.96 value is representative of clear atmospheric conditions. Charlock and Sellers (1980) established a value of 0.81 for an atmosphere that was neither warming nor cooling. The 0.65 value is a lower limit for dust-like material (Whitlock et al. 1985). The lowest value, 0.50, is more typical of an urban aerosol (Whitlock et al. 1985) or soot (Hansen et al. 1980).

Figure 5 is a plot of the scattering phase functions for four different aerosols. The one labeled "IM.01L" was provided with the ERIM radiative transfer model and represents a typical land aerosol. It was used in all the calculations, whereas the others were selected for sensitivity studies only. (IM.01L signifies that the imaginary part of the refractive index (i.e., absorption coefficient) is equal to 0.01, and L signifies land aerosol. Model No. 25 is a model from the LOWTRAN 5 set by Kneizys et al. (1980).) An important aspect of the curves is the forward/backward scattering ratio f/b; a high ratio implies a higher atmospheric scattering component of radiance when observation is in the direction of the Sun than when observation is in the direction opposite to the Sun.

In the ERIM model, the effect of variability in the aerosol loading in the atmosphere is simulated indirectly by tying the aerosol optical thickness to the surface visual range VR through a built-in routine. The routine scales the amount of aerosol below an altitude of 5 km to an estimate of the surface visual range by decreasing the aerosol number density exponentially from the surface up to an altitude of 5 km; above 5 km a constant background amount (independent of surface VR) is used. The common meteorological visibility V is related to visual range by $\mathrm{VR} = (1.3 \pm 0.3)V$ (Kneizys et al. 1980). In our simulation VR was set equal to $(1.3 + 0.3)V$.

A more precise and meaningful way of simulating aerosol scattering is to input such optical depth values directly rather than to rely on the approximate visibility relationship. Flowers et al. (1969) have established the cumulative frequencies of daily average turbidities for three representative distributions (rural, suburban, and urban) based on the Volz aerosol turbidity parameter B. The optical thickness τ is related to turbidity by the relation $e^{-\tau} = 10^{-B}$. Thus, $\tau = 2.30259B$. The aerosol turbidity parameter B is determined by looking at the Sun with a standard photometer, at a wavelength of 0.5 μm, and correcting for the optical thickness contributions due to molecular scattering and ozone absorption. Table I gives the relations between turbidity, visual range, and visibility for the three distributions, for the 5th, 50th, and 95th percentiles. (In explanation, it should be noted that the 50th percentile is equivalent to the average condition. The 5th percentile corresponds to a quite clear atmosphere, exceeded in turbidity 95 percent of the time; the 95th percentile corresponds to a very hazy atmosphere, exceeded in turbidity only 5 percent of the time.) A rural atmosphere was used in this study, since it is believed most typical of desert environments; thus, the turbidity varied from 0.035 to 0.125 (at 0.5 μm) in the radiative transfer calculations. Turbidity values at other wavelengths are extrapolated.

Table I. Values of Turbidity B, Visual Range VR, and Visibility V for Various Percentile Values, From Flowers et al. for Three Representative Cumulative Frequency Distributions

[Estimated VR = $(1.6)V$]

Parameter	Rural	Suburban	Urban
5th percentile			
Turbidity	0.035	0.038	0.055
Visual range, km	100	97	73
Visibility, km	76	74.6	56.2
Visibility, mi	47.8	46.3	34.9
50th percentile			
Turbidity	0.063	0.094	0.175
Visual range, km	56	37	14.5
Visibility, km	43.1	28.5	11.2
Visibility, mi	26.8	17.7	6.9
95th percentile			
Turbidity	0.125	0.275	0.450
Visual range, km	26	7.6	4
Visibility, km	20	5.8	3.1
Visibility, mi	12.4	3.6	1.9

The radiative transfer computer program gives the radiance at the sensor for each set of input values.

However, when part of the surface is in shadow a separate calculation must be made. The radiance at the sensor from the shaded area is the result of scattered sunlight and is equal to

$$L(\text{indir}) = ([E(\text{tot}) - E(\text{dir})]\ \rho T/\pi) + L(\text{path})$$

Therefore, the total radiance at the sensor is a combination of L(tot) and L(indir), according to the sunlight/shadow ratio.

Results

Radiance determinations were made for an altitude of 10 km and a solar zenith angle of 75° for each of 36 possible combinations of surface reflectance, single-scattering albedo, and turbidity percentile values previously discussed. The IM.01L aerosol model was used. The sensor zenith angle and the relative azimuth angle were varied in 15° and 22.5° increments, respectively, which resulted in 46 calculations per set of input conditions. The radiance values were normalized to nadir radiance, plotted on a hemispheric grid displaying θ_r and ψ, and contoured at regular intervals. A representative set of these normalized bidirectional reflectance plots is shown in figures 6 through 11 for $\rho = 0.4$ and $\theta_s = 75°$. In figures 6 through 9, $F(B) = 50$ percent (i.e., the 50th percentile or average turbidity condition) and ω_o varies from 0.96 to 0.50. For $\omega_o = 0.81$, two additional plots are shown for $F(B)$ values of 95 percent and 5 percent in figures 10 and 11.

To compare the off-nadir reflectance variations resulting from changes in the single-scattering albedo and turbidity values, normalized reflectances in the principal plane have been plotted for surface reflectances of 0.1, 0.4, and 0.7 in figures 12, 13, and 14, respectively. The upper part of each figure is for $\omega_o = 0.96$, and the lower part is for $\omega_o = 0.50$. Each figure displays five curves: the two extreme conditions ($F(B) = 95$ percent and 5 percent) without surface shadowing and with shadowing ($H/\lambda = 0.134$), and the surface reflectance from Salomonson (1968) that was used in the computations.

Figure 15 was redrawn from Davis (1982) and shows contours of differences between the normalized reflected radiances from his study and the same quantity from the data of Salomonson (1968) for a solar zenith angle of 70° to 80°. Positive values indicate that brighter features were measured by Davis. Difference values (referred to as Δ norm. refl.) were extracted for the principal plane and used as a basis for comparison in the next four figures, which show the differences between calculated values and the Salomonson data for various input conditions.

Figure 16 shows the effect on Δ norm. refl. of variations in ω_o and ρ for a solar zenith angle of 75°, an $F(B)$ of 5 percent, and shadowing. In figure 17 the solar zenith angle is varied from 70° to 80° with constant input conditions. Figures 18 and 19 are for a solar zenith angle of 70°, a single-scattering albedo of 0.50, and aerosol model No. 25, which has a low forward/backward scattering ratio. Figure 18 illustrates the influence of shadowing variations for $F(B)$ values of 5 percent and 50 percent, for $\rho = 0.4$, while figure 19 gives the same for $\rho = 0.7$.

Discussion

Aerosols

Figures 6 through 9 illustrate the effect of the single-scattering albedo on reflectance measurements at high altitude. With no intervening atmosphere, these hemispheric plots should look like the Salomonson data in figure 3, which was used as the input to the program. Scattering and absorption, however, have caused a distortion in the reflectance, particularly along the principal plane. The highest scattering value ($\omega_o = 0.96$) introduced the greatest error in the measurement because of the increased path radiance at high zenith angles. In figures 10 and 11, where the single-scattering albedo is constant and the turbidity is varied, the higher turbidity produced the most distortion in the reflectance pattern because of the increased path radiance. There are other factors that could also influence these reflectance plots, but they will be discussed later when comparisons are made with the data from Davis.

Notice that the reflectance plots, although distorted by the atmosphere, still resemble the Salomonson data. The reflectance data from Davis presented in figure 15 shows more detail, especially at nadir, than the original Salomonson data. These features may be real or an artifact of the measurements. Since Davis collected data in only 12 off-nadir directions at angles of either 30° or 60°, and then performed a harmonic analysis to generate the final bidirectional reflectance plot, the variations at nadir are considered to be artificial. On the other hand, they may have been suppressed in the data presented here by the scattering phase function entered into the program and/or the simplifications used in the radiative transfer calculations within the program.

Because of the subtle differences in the normalized reflectances when the atmospheric and surface conditions are varied, comparisons of the data are best shown in the principal plane. From the plots displayed in figures 12 through 14, four general observations can be made. First, an increase in turbidity increases the normalized reflectances at high

zenith angles, particularly when looking in the direction of the Sun ($\psi = 0°$). This increase is primarily due to the increased atmospheric path length relative to nadir and to the fact that the aerosol phase function is peaked in the forward direction and to a lesser extent in the backward direction (see fig. 5), which causes the path radiance to be more pronounced. Second, a decrease in the single-scattering albedo tends to reduce the relative atmospheric effect at high zenith angles, which results in a lower normalized reflectance. This decrease is brought about by an increase in the aerosol absorption, which has a more pronounced effect over the longer path length. Third, when the surface reflectance is increased, the normalized reflectances at high zenith angles are reduced. In this case the normalizing effect of the higher nadir radiance, which increases directly with surface reflectance, is responsible. And fourth, the surface shadowing effect tends to decrease the normalized reflectance in the $\psi = 0°$ direction and increase it in the $\psi = 180°$ direction. Since shadowing has reduced the radiances continuously from the $\psi = 180°$direction to the $\psi = 0°$ direction, the net effect is to decrease the radiance relative to nadir in the $\psi = 0°$ direction and to increase the radiance relative to nadir in the $\psi = 180°$ direction.

Although the above trends in the data were generally anticipated, it is the magnitudes of the effects that are most important. Several of the normalized reflectance curves show a decrease in reflectance relative to the surface in the $\psi = 0°$ direction. Since the Davis data also behave in this manner, it is meaningful to note those conditions that enhance this effect. It is seen that low turbidity, low single-scattering albedo, high surface reflectance, and shadowing are generally favorable to a reduction in the normalized reflectance. These variables, along with several others, will next be manipulated in the input parameters in an attempt to reproduce the results of Davis.

Davis Flight Data

In figures 16 through 19 several input parameters were varied and the results compared with those of Davis. Figure 16, which illustrates the effect of varying surface reflectance for two single-scattering albedo conditions, shows that the more absorbing atmosphere and the higher reflectance surface produced the most favorable results. In figure 17 the most favorable turbidity (5 percent) and single-scattering albedo (0.50) conditions were held constant, and the solar zenith angle was varied. The zenith angle of 70° gave the best results in the $\psi = 0°$ direction but least favorable in the $\psi = 180°$ direction because of the highly peaked scattering phase function. Decreasing the sensor-surface-Sun angle, by elevating the Sun, reduced the path radiance relative to nadir, and thus depressed both ends of the curve.

In figure 18 the effect of varying two new parameters is illustrated. The aerosol phase function has been changed with the use of LOWTRAN 5 model No. 25 (which has a low f/b) shown in figure 5, and the shadowing has been further increased to $H/\lambda = 0.2$. With the solar zenith angle equal to 70°, the three shadowing values of 0.1, 0.134, and 0.2 give 28, 37, and 55 percent shadow at nadir, respectively. Increasing the shadowing reduced the reflectance in the $\psi = 0°$ direction and increased it in the $\psi = 180°$ direction. The curve for $H/\lambda = 0.134$ from figure 17 lies between the two extremes in figure 18. Although the new aerosol model has changed the shape of these curves somewhat, the major influence has been to reduce the extreme values in the $\psi = 0°$ direction. Increasing the surface reflectance in figure 19 had only a small effect on the results.

The variation in Davis' data at nadir can be approximated by varying the surface reflectance across the field of view: for instance, by letting $\rho = 0.4$ in the $\psi = 0°$ direction and $\rho = 0.7$ in the $\psi = 180°$ direction, with the nadir reflectance being an average of the two values (i.e., 0.55). Although such a change in surface reflectance is physically possible, it does not seem reasonable for data collected during a solar zenith angle variation of 10°. As mentioned before, this feature of Davis' data is thought to be an artifact resulting from the mathematical harmonic analysis of limited data.

It is clear in the simulation of Davis' data that the values of the atmospheric parameters are not what one would expect during the summer monsoon season. Indeed, some of them are quite unrealistic, such as a very clear atmospheric condition with a low value of single-scattering albedo. In the following section, a discussion will be given concerning a viable range of environmental parameters for desert areas.

Desert Environments

There are several good sources of information concerning desert environmental conditions. However, none of them give all of the parameters necessary to adequately describe the radiative transfer conditions. For the purpose of this discussion, six important variables will be reviewed; they are aerosol distribution, optical depth, single-scattering albedo, scattering phase function, surface reflectance, and shadowing.

Patterson and Grams (1981) investigated the haze over the Saudi Arabian peninsula and the Arabian Sea during the summer monsoon season and

found that the aerosol layer extended from the surface to an altitude of approximately 6 km over the desert regions. (It should be noted here that the Patterson and Grams data and the Davis data were collected 2 years apart.) Over both areas the highest concentrations were near the surface, and there was an indication of layering. There was not one well-mixed layer extending from the surface to the top of the haze, but multiple layers. In both of these cases, the concentration actually decreased at the lowest level measured, which implies that the source of the aerosol was not directly below the measurement location and suggests that transport from some distant source was important. The layering also suggests the possibility of multiple sources for the haze layers. Schutz and Sebert (1984) also found this transport condition to be characteristic of the Saharan dust layer.

As previously mentioned, the Turner program used in this study assumes a well-mixed aerosol layer with an exponential decrease from the surface to an altitude of 5 km. This aspect of the program is considered to have a minor influence on the results, however, since the aerosol effects are usually variable with time and distance and are difficult to model. A more important parameter is the optical depth, which integrates the effect of the total aerosol burden.

In a review of global atmospheric aerosols, Toon and Pollack (1976) referenced an optical depth over Israel of $\tau = 0.24$ when dust is blown from the North African deserts. For the Saudi Arabian peninsula, Patterson and Grams (1981) described the visibility as less than 10 km and assumed an optical depth of approximately 1.5. Although these two conditions at first glance do not seem to be compatible with table I (that is, a visibility of 3 km represents an optical depth of only 1.2), it should be remembered that the aerosol density actually decreased near the surface, which permitted a higher visibility than suggested by the optical depth. Endemann et al. (1984) developed an aerosol model that was thought to be typical of a heavy haze in desert areas of the world, especially in spring and summer. The continental-type boundary layer extended up to 6 km and had an optical depth of 3.3. This value exceeds the boundaries of the turbidity models that were established by Flowers et al. (1969) for the United States and were used in this study.

The optical effects of the aerosols, which include the single-scattering albedo and the scattering phase function, are determined by the complex index of refraction, the size distribution, and the shape of the aerosol particles. The complex index of refraction $n = n_{\mathrm{re}} - in_{\mathrm{im}}$ consists of a real part n_{re}, which is the ratio of the velocity of light in a vacuum to the velocity of light in the material, and an imaginary part n_{im}, which is an absorption parameter characterizing the material. Patterson et al. (1977) and Patterson (1981) have evaluated the optical properties of crustal aerosols and found for visible wavelengths that n_{re} lies between 1.5 and 1.6 and n_{im} lies between 0.001 and 0.1. The real part controls scattering whereas the imaginary part determines aerosol absorption. By assuming that the particles are spherical, the Mie theory (see Bohren and Huffman, 1983) can be used to determine the interaction of the particles with the radiation field. A number of authors have constructed aerosol models and used the Mie theory to define the optical effects.

Braslau and Dave (1973a and b) have studied aerosols with an imaginary refractive index of 0.01 and found that ω_o was about 0.9. Patterson and Grams (1981) considered the Saudi Arabian desert haze with an optical depth of 1.5 and determined an atmospheric absorption of about 15 percent; i.e., $\omega_o = 0.85$. Minnis and Cox (1978) found that dust in the Saharan air layer could cause increases in the fractional absorption of the atmosphere from 4 percent to 19 percent.

In their study of the Arabian peninsula aerosol layer, Patterson and Grams noticed a highly absorptive background material, assumed to be carbon, above the haze layer. The effect this material has on the optical properties of the aerosol layer will depend on its concentration. The desert aerosol model of Endemann et al. (1984) contained 1 percent soot and had an ω_o of 0.88. Their urban-industrial haze model was composed of 22 percent soot with $\omega_o = 0.64$. Bohren and Huffman (1983) calculated the effect of an addition of 1 percent soot to an aerosol model with two different techniques. In the first case the small soot particles were mixed with the larger (1.5 μm) particles, and in the second case the soot was imbedded in the larger particles. The imbedding technique enhanced the effectiveness of the absorption of the soot and decreased ω_o from about 0.9 to 0.75. This method of mixing could be very important in the event that volatile aerosols are present and not recovered in the sampling procedure.

The aerosol-scattering phase function, which is wavelength dependent, usually has a maximum in the forward direction, a lesser maximum in the backward direction, and a minimum between 90° to 120°. According to Barteneva (1960) the phase function is nearly flat for a very clear atmosphere and gradually becomes more forward scattering as the turbidity increases. Kneizys et al. (1980) have developed 70 aerosol-scattering phase functions that are considered to be representative of various aerosol models

and wavelengths. Model No. 25, used in this report, has a slightly higher forward/backward scattering ratio than a very clear atmosphere but much less than the phase functions used in their tropospheric models. (It is important to note that when multiple scattering becomes important, such as in a dense cloud, the surface tends to become more diffuse, which reduces the effect of a high f/b ratio.) In the visible region, the forward/backward scattering ratio of common land aerosols can vary from about 40 to over 400.

The reflectance of the White Sands target was described as the most isotropic target investigated by Salomonson. For higher solar elevation angles, the principal plane reflectance showed only a slight increase in the $\psi = 180°$ direction and essentially no increase in the $\psi = 0°$ direction. As the solar zenith angle increased, the reflectance increased somewhat in the $\psi = 180°$ direction and even more in the $\psi = 0°$ direction. The increase in the $\psi = 0°$ direction is taken to be due to specular reflectance. For those desert surfaces with vegetation, the reflectance increased back toward the Sun (in the $\psi = 180°$ direction) and decreased away from the Sun. This occurrence can be described qualitatively as a shadow effect that appears to be related to the size of the elements creating the reflection. In the reflectances of the dry desert lake bed and the salt plain surfaces, shown in figure 1, the small humps between nadir and the solar zenith angle are related to the "hot spot", i.e., the point where the Sun-sensor line intersects the surface. In laboratory measurements the hot spot was located at the solar zenith angle, whereas the displacement in the field was thought to result from a more diffuse illumination condition (Salomonson, 1968).

Although shadowing is an integral part of the reflectance mechanism of most natural surfaces, it is essential to consider the influence of larger features not generally accounted for in field measurements. Rocks, boulders, dunes, hills, and even mountains can be important to the scene reflectance when viewed from high altitude. Landsat images of the Arabian peninsula (Short et al., 1976) reveal a variety of dune types and mountainous terrain where shadowing is clearly evident even with a relatively small solar zenith angle. In a review of regional landforms, Short and Blair (1986) noted eolian features with heights of 50 to 150 m and wavelengths of 500 m to 3 km; these could account for about one-half of the shadowing in the nominal case ($H/\lambda = 0.134$) used in this study.

In closing the discussion on desert environments, it is apparent that the uncertainties in the scattering function, single-scattering albedo, and turbidity, even under favorable conditions, preclude the selection of a most probable set of these parameters for the radiation transfer study. However, one parameter that has a significant effect on Davis' data and is independent of these atmospheric parameters is the surface reflectance. The reflectance model chosen contains a specular reflectance component that has constrained the choice of atmospheric turbidity for the simulation of Davis' flight data. Salomonson remarks that the most likely principal plane reflectance curve for sand would have a minimum near nadir and would increase toward the Sun. Removing the specular component from Salomonson's data and introducing a shadowing factor would permit a more reasonable choice of aerosol conditions for the comparison with Davis' results.

Concluding Remarks

A review of atmospheric conditions for desert areas has revealed that environmental parameters can be highly variable, which makes it difficult to establish an average condition for radiative transfer simulations. In this study concerning the influence of aerosols on the remote sensing of surface reflectances, a rural atmospheric condition (Flowers et al., 1969) was assumed to be typical of North American deserts. A desert reflectance for a high solar zenith angle, taken from Salomonson (1968), was used as the surface reflectance model. With a suitable choice of input values for the modeling program, it was possible to approximate the flight results of Davis (1982) for the Saudi Arabian desert. The assumed low turbidity conditions did not seem reasonable, however, particularly for that region of the globe during the summer monsoon season. It was concluded that a different surface reflectance model, e.g., one without a specular component and with some shadowing, would have permitted a more realistic choice of modeled atmospheric conditions and should have given a closer match to the observed reflectance curves.

NASA Langley Research Center
Hampton, Virginia 23665-5225
August 5, 1987

References

Ashburn, Edward V.; and Weldon, Rodney G.: Spectral Diffuse Reflectance of Desert Surfaces. *J. Opt. Soc. America*, vol. 46, no. 8, Aug. 1956, pp. 583–586.

Barteneva, O. D.: Scattering Functions of Light in the Atmospheric Boundary Layer. *Bull. (Izvestiya), Academy of Sciences, USSR, Geophysics Ser.*, no. 12, Dec. 1960, pp. 1237–1244.

Bohren, Craig F.; and Huffman, Donald R.: *Absorption and Scattering of Light by Small Particles.* John Wiley & Sons, Inc., c.1983.

Bowker, David E.; Davis, Richard E.; Myrick, David L.; Stacy, Kathryn; and Jones, William T.: *Spectral Reflectances of Natural Targets for Use in Remote Sensing Studies.* NASA RP-1139, 1985.

Bowker, D. E.; Davis, R. E.; Von Ofenheim, W. H. C.; and Myrick, D. L.: Estimation of Spectral Reflectance Signatures From Spectral Radiance Profiles. *Proceedings of the Seventeenth International Symposium on Remote Sensing of Environment,* Volume II, Environmental Research Inst. of Michigan, 1983, pp. 795–814.

Braslau, Norman; and Dave, J. V.: Effect of Aerosols on the Transfer of Solar Energy Through Realistic Model Atmospheres. Part I: Non-Absorbing Aerosols. *J. Appl. Meteorol.*, vol. 12, no. 4, June 1973a, pp. 601–615.

Braslau, Norman; and Dave, J. V.: Effect of Aerosols on the Transfer of Solar Energy Through Realistic Model Atmospheres. Part II: Partly-Absorbing Aerosols. *J. Appl. Meteorol.*, vol. 12, no. 4, June 1973b, pp. 616–619.

Charlock, Thomas P.; and Sellers, William D.: Aerosol Effects on Climate: Calculations With Time-Dependent and Steady-State Radiative-Convective Models. *J. Atmos. Sci.*, vol. 37, no. 6, June 1980, pp. 1327–1341.

Cooper, Kevin D.; and Smith, James A.: A Monte Carlo Reflectance Model for Soil Surfaces With Three-Dimensional Structure. *IEEE Trans. Geosci. & Remote Sens.*, vol. GE-23, no. 5, Sept. 1985, pp. 668–673.

Davis, J. M.: Regionally Applicable Angular Reflectance Models. *Earth Radiation Science Seminars,* John B. Hall, Jr., compiler, NASA CP-2239, 1982, pp. 45–51.

Endemann, M.; Grassl, H.; Schlussel, P.; Labitzke, K.; Quenzel, H.; Thomalla, E.; and Nodop, K.: *Orbiting Lidars for Atmospheric Sounding—Final Report, Volume 1.* ESA-CR(P)-2112-VOL-1 (BLEV-R-65.498-5-VOL-1) (ESTEC Contract No. 5186/82/NL/HP), Battelle-Institut e.V. Frankfurt am Main (Federal Republic of Germany), Dec. 1984.

Fitch, Bruce W.: Effects of Reflection by Natural Surfaces on the Radiation Emerging From the Top of the Earth's Atmosphere. *J. Atmos. Sci.*, vol. 38, no. 12, Dec. 1981, pp. 2717–2729.

Flowers, E. C.; McCormick, R. A.; and Kurfis, K. R.: Atmospheric Turbidity Over the United States, 1961–66. *J. Appl. Meteorol.*, vol. 8, no. 6, Dec. 1969, pp. 955–962.

Fraser, Robert S.; and Kaufman, Yoram J.: The Relative Importance of Aerosol Scattering and Absorption in Remote Sensing. *Fifth Conference on Atmospheric Radiation,* American Meteorological Soc., c.1983, pp. 98–102.

Hansen, James E.; Lacis, Andrew A.; Lee, Pauthon; and Wang, Wei-Chyung: Climatic Effects of Atmospheric Aerosols. *Aerosols: Anthropogenic and Natural, Sources and Transport,* Theo J. Kneip and Paul J. Lioy, eds., New York Academy of Sciences, 1980, pp. 575–587.

Kimes, D. S.; Newcomb, W. W.; Tucker, C. J.; Zonneveld, I. S.; Van Wijngaarden, W.; De Leeuw, J.; and Epema, G. F.: Directional Reflectance Factor Distributions for Cover Types of Northern Africa. *Remote Sens. Environ.*, vol. 18, no. 1, Aug. 1985, pp. 1–19.

Kimes, D. S.; and Sellers, P. J.: Inferring Hemispherical Reflectance of the Earth's Surface for Global Energy Budgets From Remotely Sensed Nadir or Directional Radiance Values. *Remote Sens. Environ.*, vol. 18, no. 3, Dec. 1985, pp. 205–223.

Kneizys, F. X.; Shettle, E. P.; Gallery, W. O.; Chetwynd, J. H., Jr.; Abreu, L. W.; Selby, J. E. A.; Fenn, R. W.; and McClatchey, R. A.: *Atmospheric Transmittance/Radiance: Computer Code LOWTRAN 5.* AFGL-TR-80-0067, U.S. Air Force, Feb. 21, 1980. (Available from DTIC as AD A088 215.)

Minnis, Patrick; and Cox, Stephen K.: *Magnitude of the Radiative Effects of the Saharan Dust Layer.* CSU ATSP-283 (Grants OCD 74-21678 and ATM 77-15369), Colorado State Univ., Jan. 1978. (Available from NTIS as PB 286 835.)

Norman, John M.; Welles, Jon M.; and Walter, Elizabeth A.: Contrasts Among Bidirectional Reflectance of Leaves, Canopies, and Soils. *IEEE Trans. Geosci. & Remote Sens.*, vol. GE-23, no. 5, Sept. 1985, pp. 659–667.

Patterson, E. M.: Optical Properties of the Crustal Aerosol: Relation to Chemical and Physical Characteristics. *J. Geophys. Res.,* vol. 86, no. C4, Apr. 20, 1981, pp. 3236–3246.

Patterson, E. M.; and Grams, G. W.: Measurements of Aerosol Radiative Properties During MONEX: Implications of the Measurements for Radiative Heating Rates. *International Conference on Early Results of FGGE and Large-Scale Aspects of Its Monsoon Experiments—Condensed Papers and Meeting Report,* World Meteorological Organization, 1981, pp. 6-40–6-43.

Patterson, E. M.; Gillette, D. A.; and Stockton, B. H.: Complex Index of Refraction Between 300 and 700 nm for Saharan Aerosols. *J. Geophys. Res.,* vol. 82, no. 21, July 20, 1977, pp. 3153–3160.

Salomonson, V. V.: Anisotropy in Reflected Solar Radiation. Ph.D. Thesis, Colorado State Univ., 1968.

Schutz, L.; and Sebert, M.: Mineral Aerosols and Source Identification. *Eleventh International Conference on Atmospheric Aerosols, Condensation and Ice Nuclei,* Volume 1, International Commission for Cloud Physics/ Committee on Nucleation, Sept. 1984, pp. 123–127. (Available from NTIS as PB85 182 400.)

Short, Nicholas M.; and Blair, Robert W., Jr., eds.: *Geomorphology From Space—A Global Overview of Regional Landforms.* NASA SP-486, 1986.

Short, Nicholas M.; Lowman, Paul D., Jr.; Freden, Stanley C.; and Finch, William A., Jr.: *Mission to Earth: Landsat Views the World.* NASA SP-360, 1976.

Staylor, W. Frank: *Site Selection and Directional Models of Deserts Used for ERBE Validation Targets.* NASA TP-2540, 1986.

Toon, Owen B.; and Pollack, James B.: A Global Average of Atmospheric Aerosols for Radiative Transfer Calculations. *J. Appl. Meteorol.,* vol. 15, no. 3, Mar. 1976, pp. 225–246.

Turner, Robert E.: *Radiative Transfer in Real Atmospheres.* ERIM 190100-24-T (Contract NAS9-9784), Infrared and Optics Div., Environmental Research Institute of Michigan, July 1974. (Available as NASA CR-140199.)

Whitlock, Charles H.; Suttles, John T.; and LeCroy, S. R.: *Phase Function, Backscatter, Extinction, and Absorption for Standard Radiation Atmosphere and El Chichon Aerosol Models at Visible and Near-Infrared Wavelengths.* NASA TM-86379, 1985.

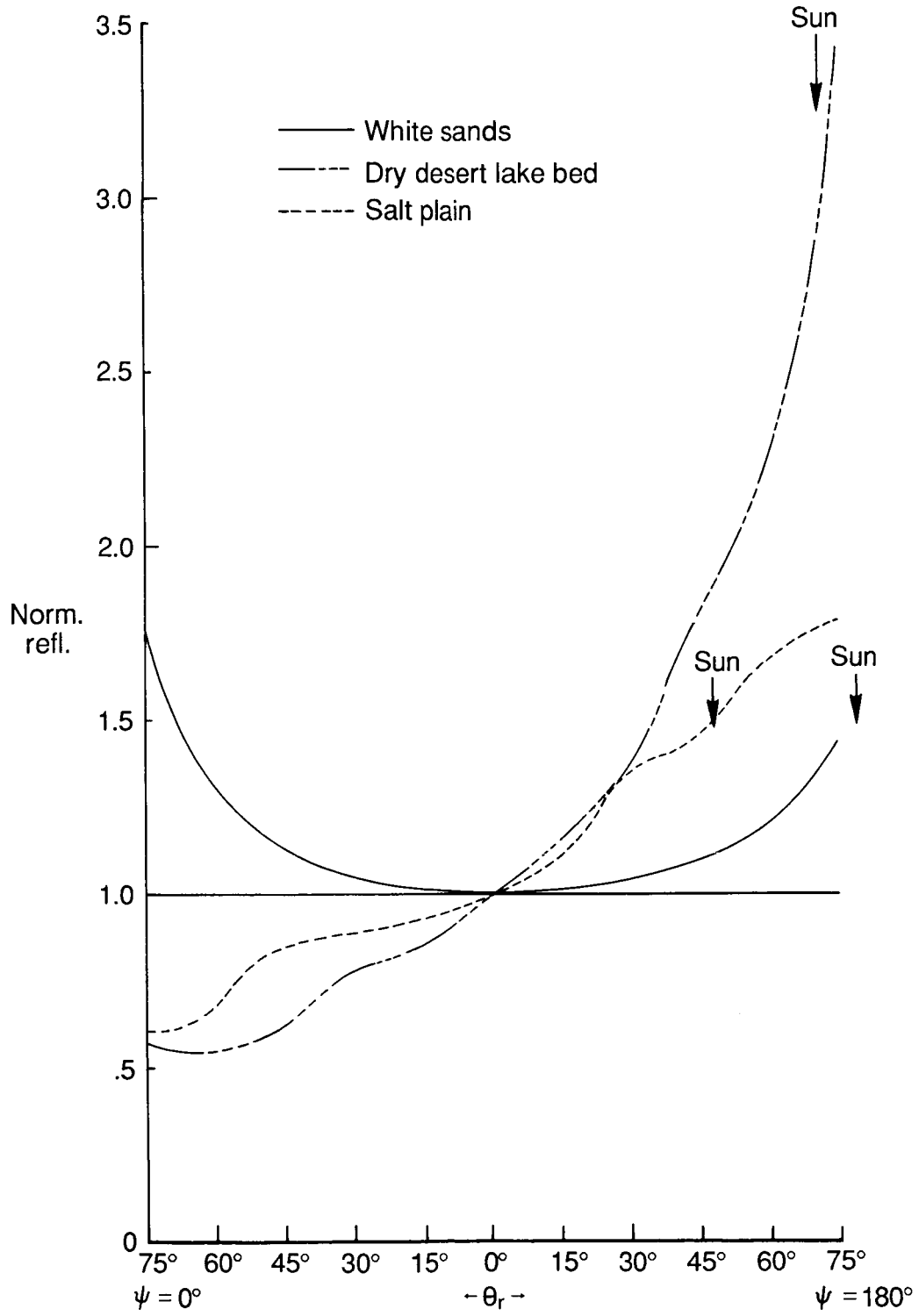

Figure 1. Normalized reflectances in the principal plane for three typical desert surfaces: white sand and dry desert lake bed (Salomonson, 1968), and salt plain (Kimes et al., 1985). The solar zenith angle is shown for each plot.

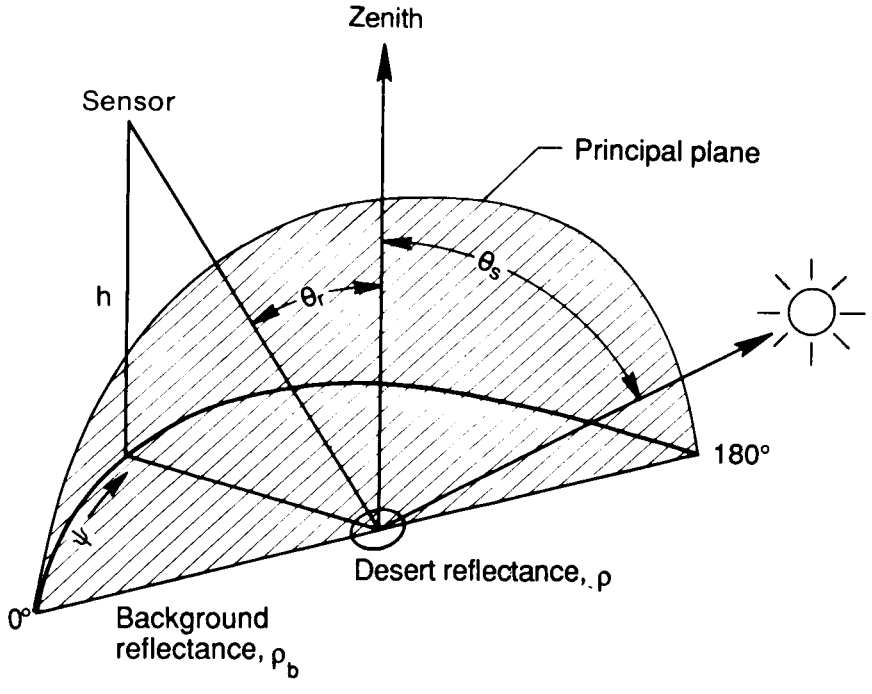

Figure 2. Viewing geometry for BRF measurements.

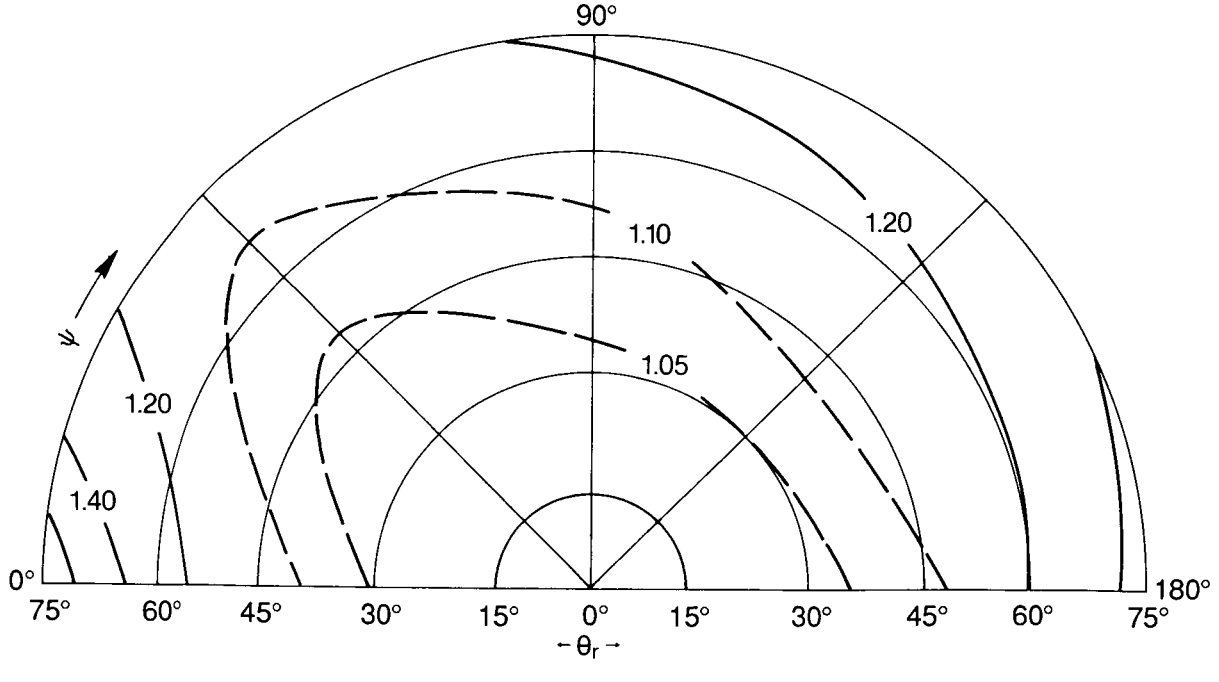

Figure 3. Normalized BRF plot for white sand, from Salomonson (1968). The solar zenith angle varied from 76° to 82°.

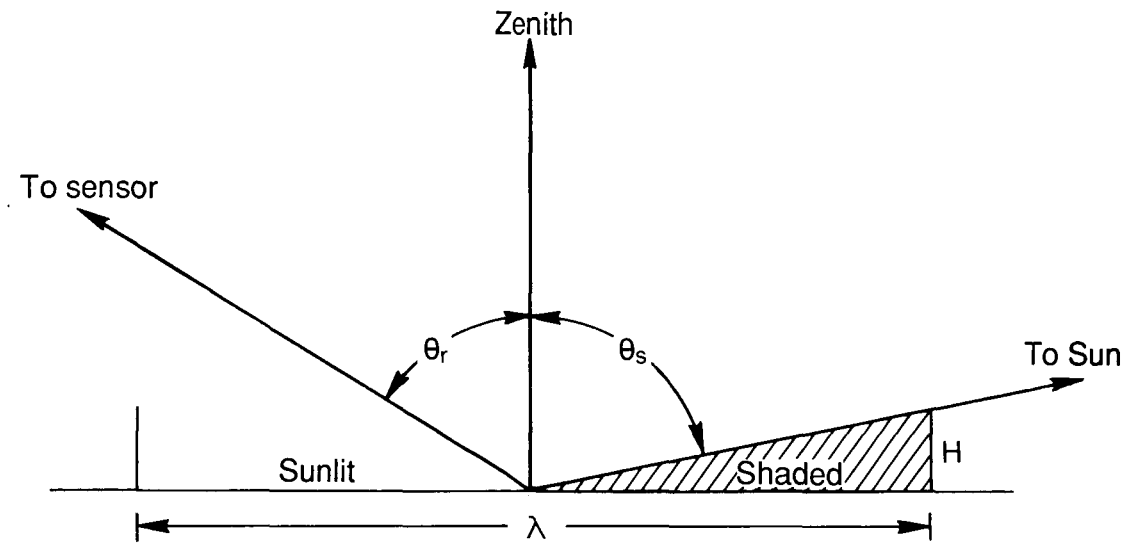

$$\frac{\text{Shaded area}}{\text{Total area}} = \frac{H}{\lambda}\,(\tan\theta_s + \tan\theta_r)\,\Big|_{\psi = 0°}$$

$$= \frac{H}{\lambda}\,(\tan\theta_s - \tan\theta_r)\,\Big|_{\psi = 180°}$$

Figure 4. Illustration of the shadowing model used in the radiative transfer calculations for the principal plane; the height H of a repetitive surface feature with wavelength λ is shown. The feature is assumed to be continuous and perpendicular to the paper.

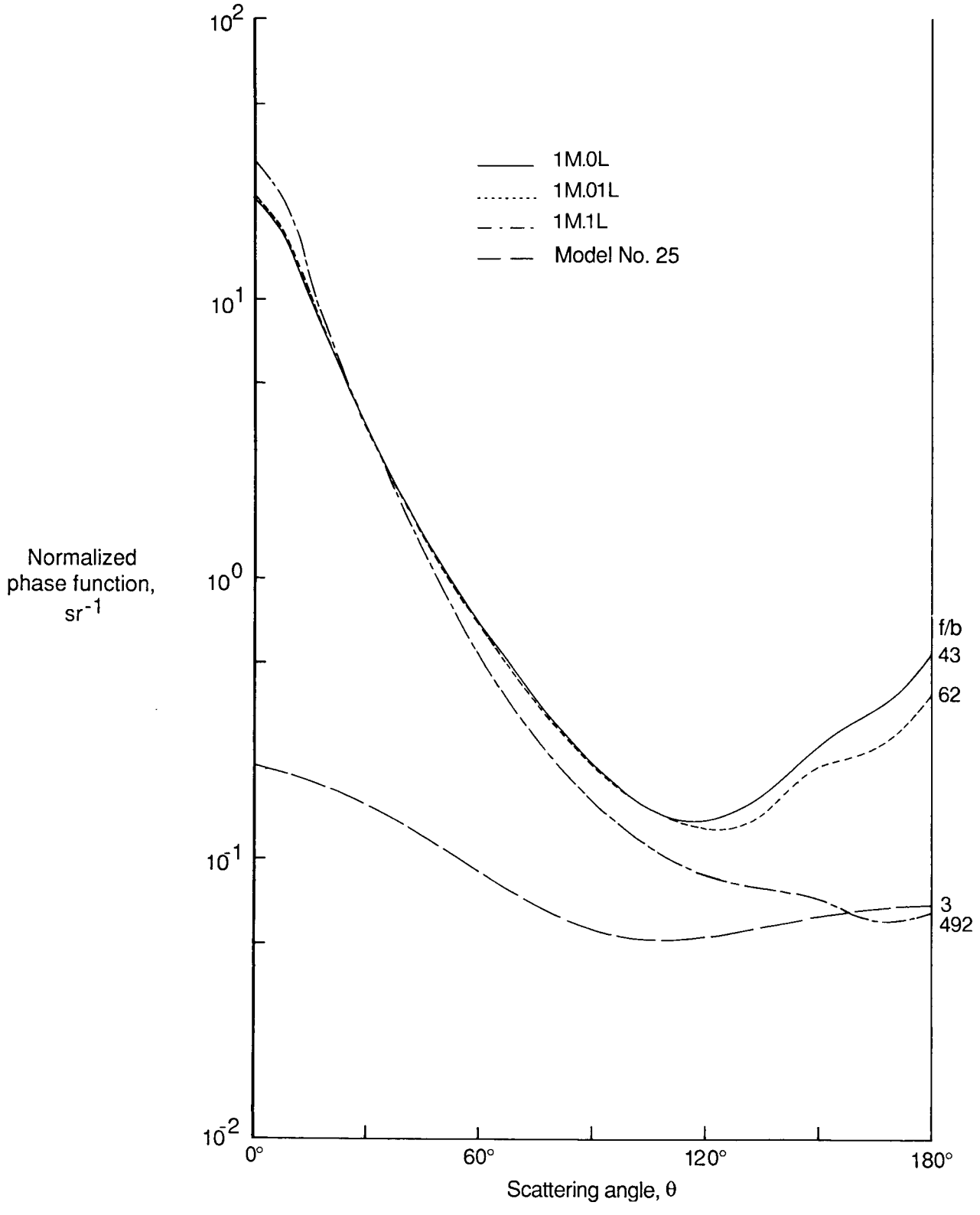

Figure 5. The normalized scattering phase functions for four aerosol models used in the radiative transfer calculations.

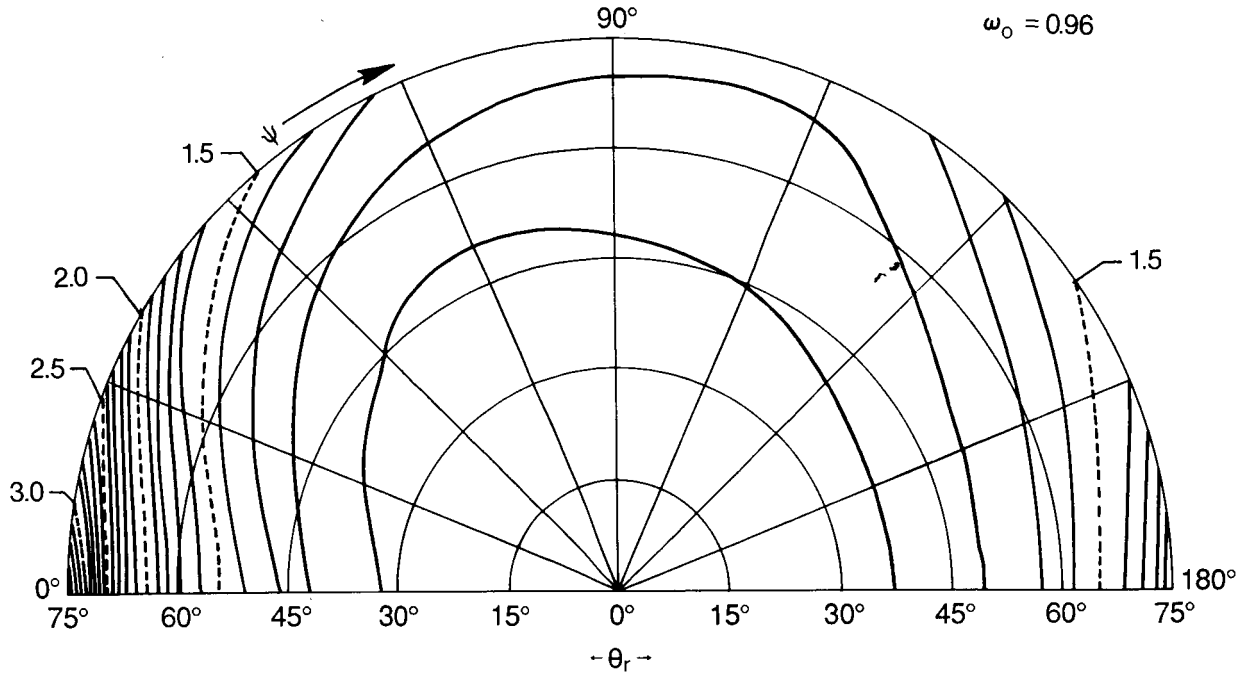

Figure 6. Normalized BRF plot for desert surface with $\rho = 0.4$, $\omega_o = 0.96$, $F(B) = 50$ percent, and $\theta_s = 75°$. Calculations for all figures are for $\lambda = 0.7\mu$m and $h = 10$ km.

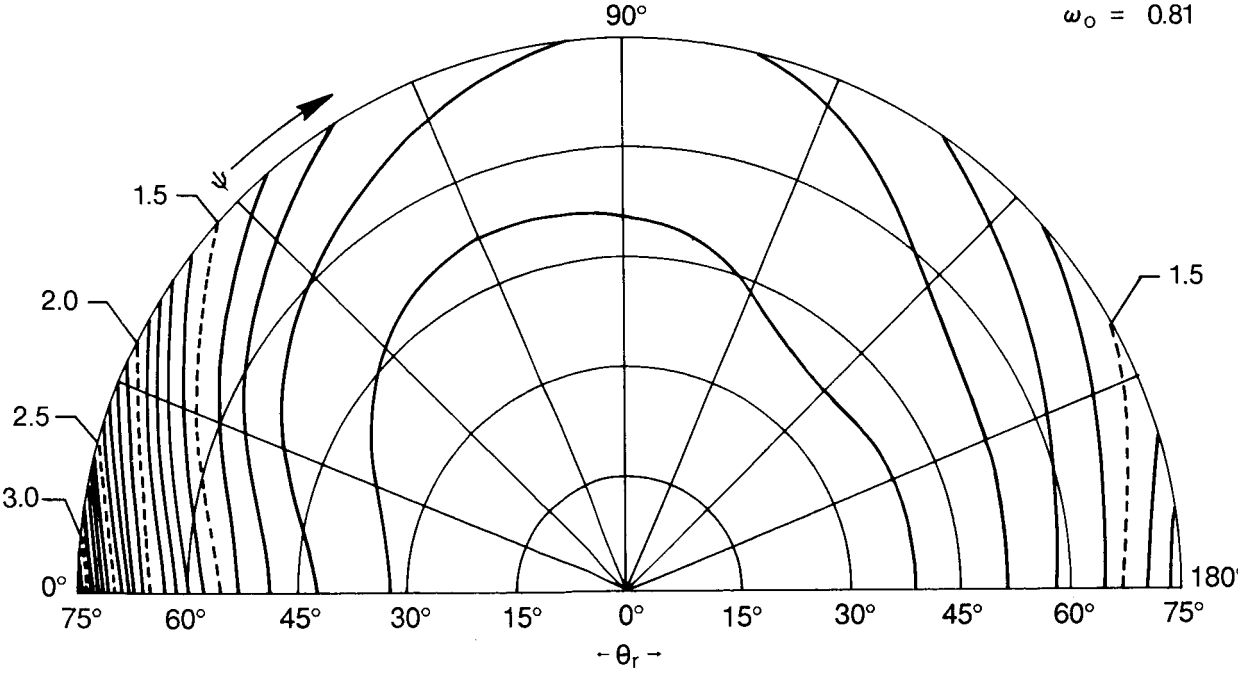

Figure 7. Normalized BRF plot for desert surface with $\rho = 0.4$, $\omega_o = 0.81$, $F(B) = 50$ percent, and $\theta_s = 75°$.

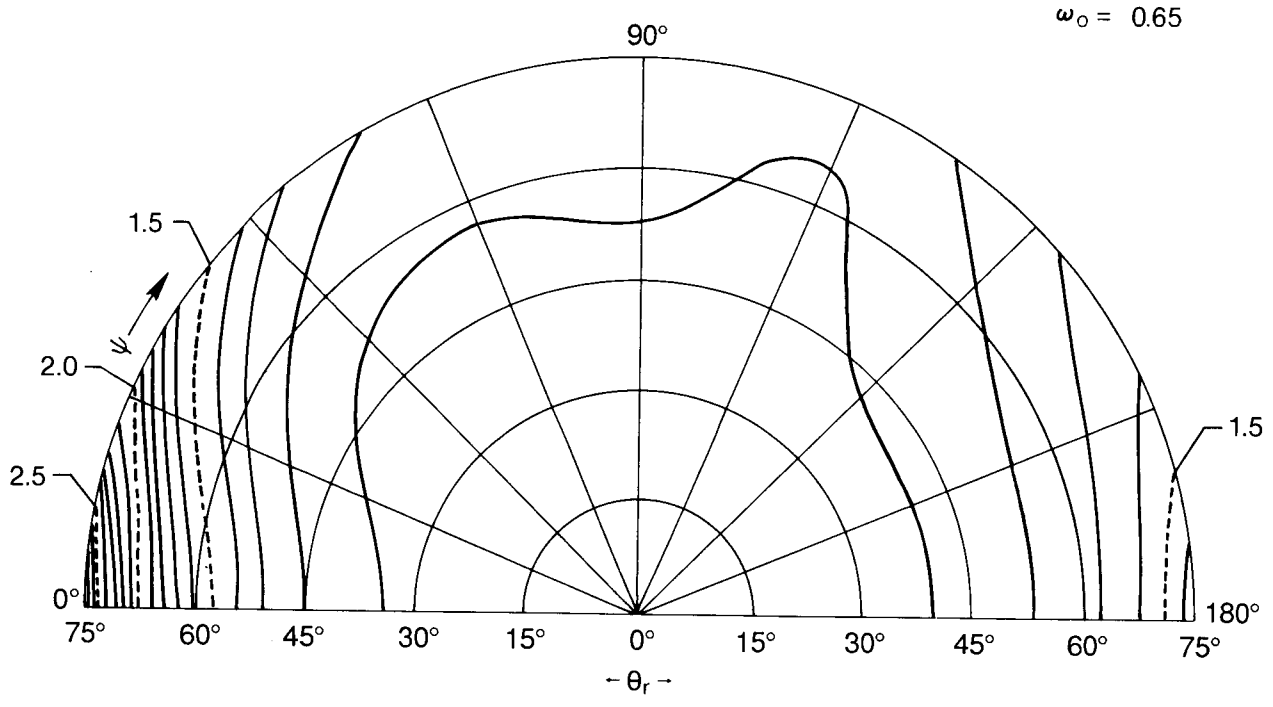

Figure 8. Normalized BRF plot for desert surface with $\rho = 0.4$, $\omega_o = 0.65$, $F(B) = 50$ percent, and $\theta_s = 75°$.

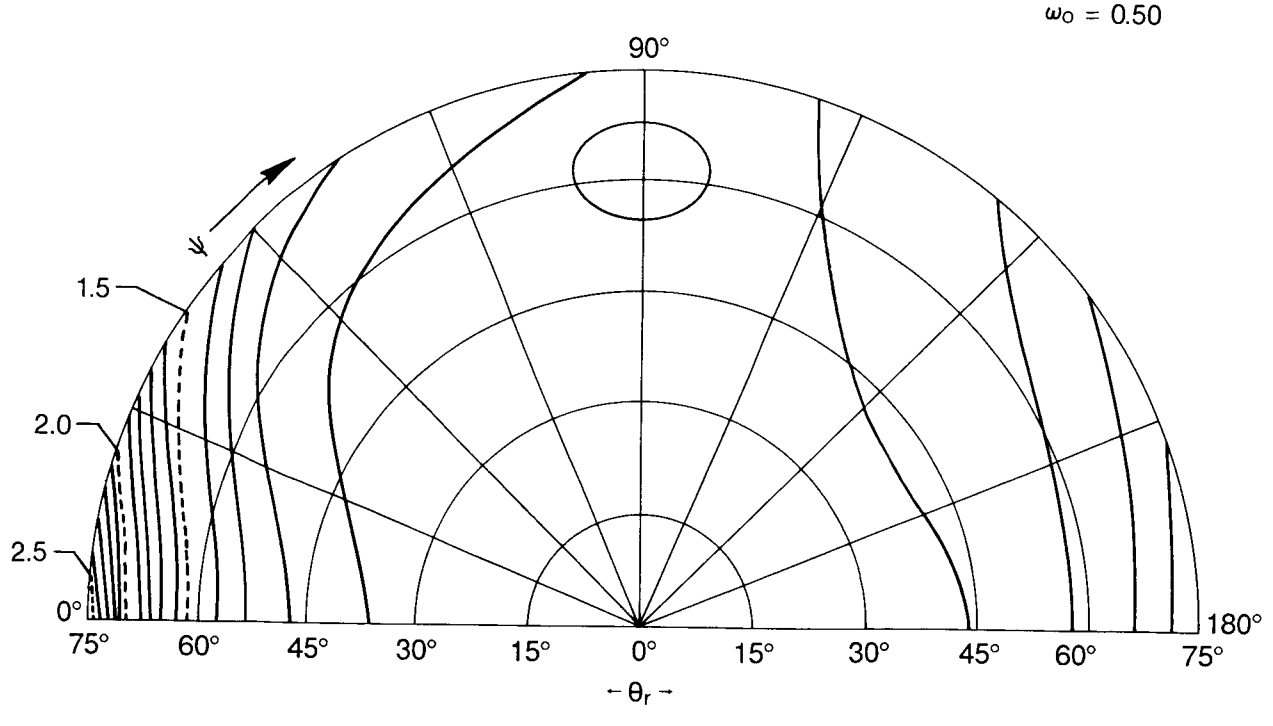

Figure 9. Normalized BRF plot for desert surface with $\rho = 0.4$, $\omega_o = 0.81$, $F(B) = 50$ percent, and $\theta_s = 75°$.

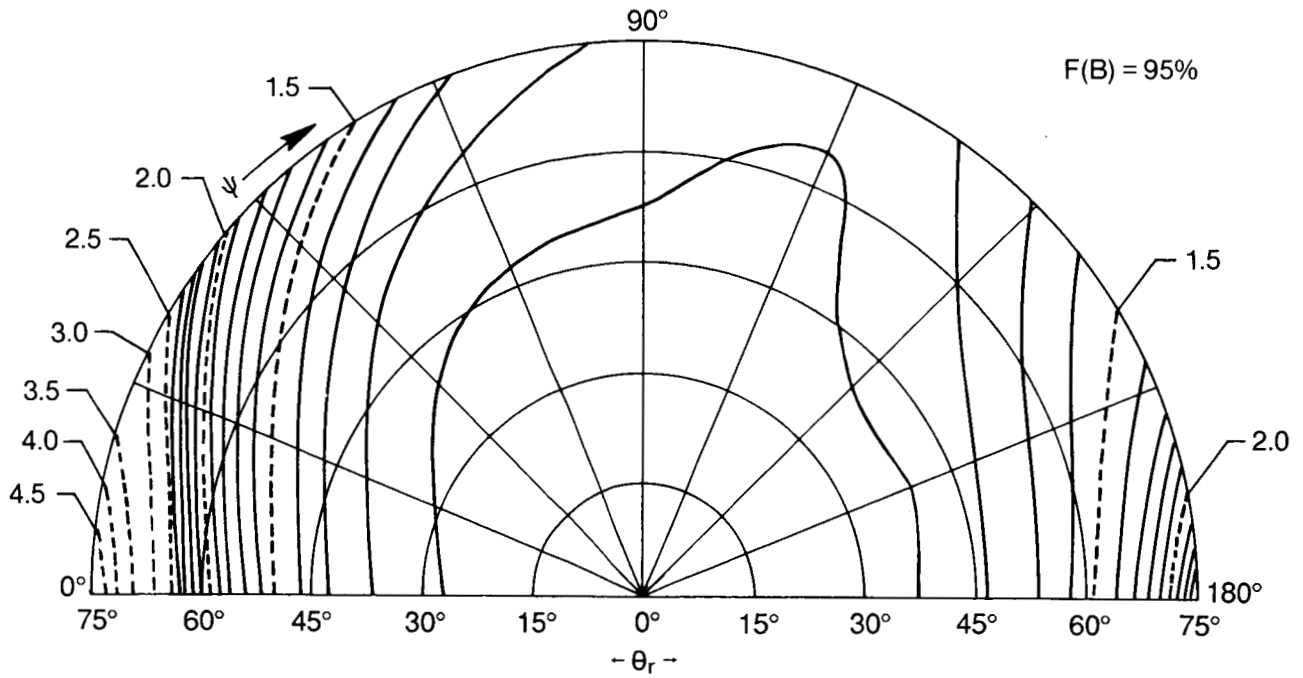

Figure 10. Normalized BRF plot for desert surface with $\rho = 0.4$, $\omega_o = 0.81$, $F(B) = 95$ percent, and $\theta_s = 75°$.

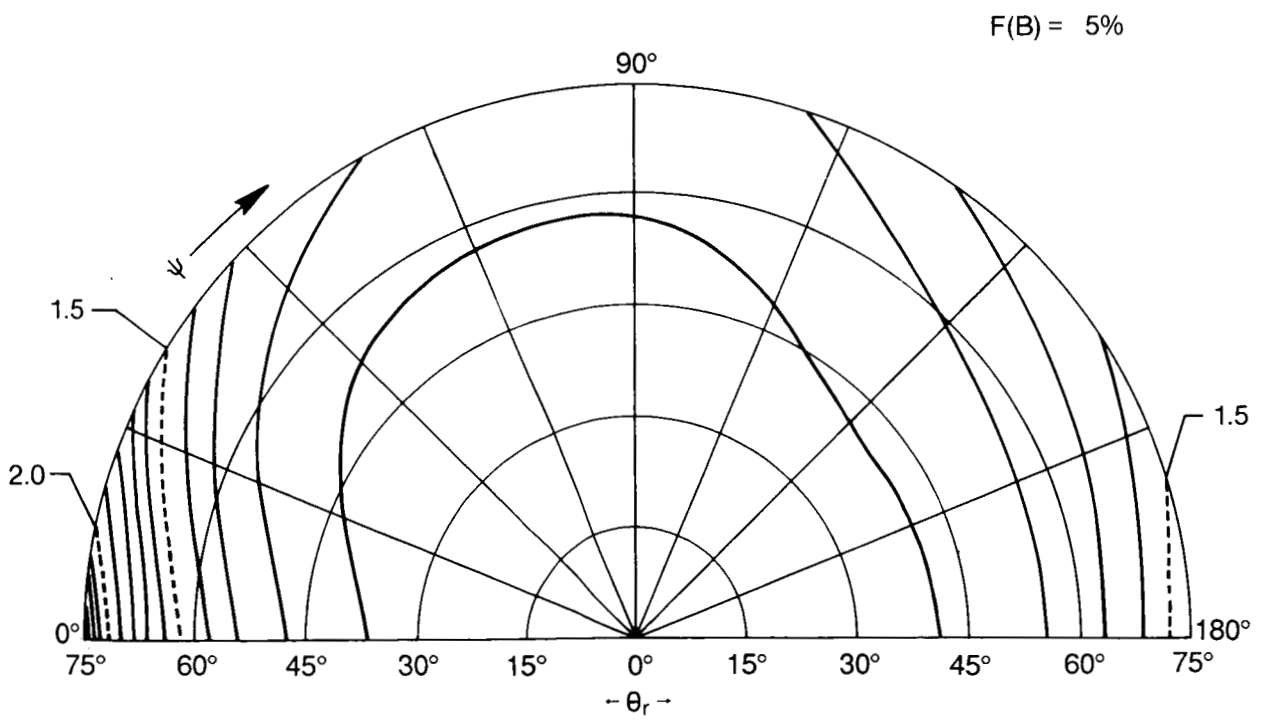

Figure 11. Normalized BRF plot for desert surface with $\rho = 0.4$, $\omega_o = 0.81$, $F(B) = 5$ percent, and $\theta_s = 75°$.

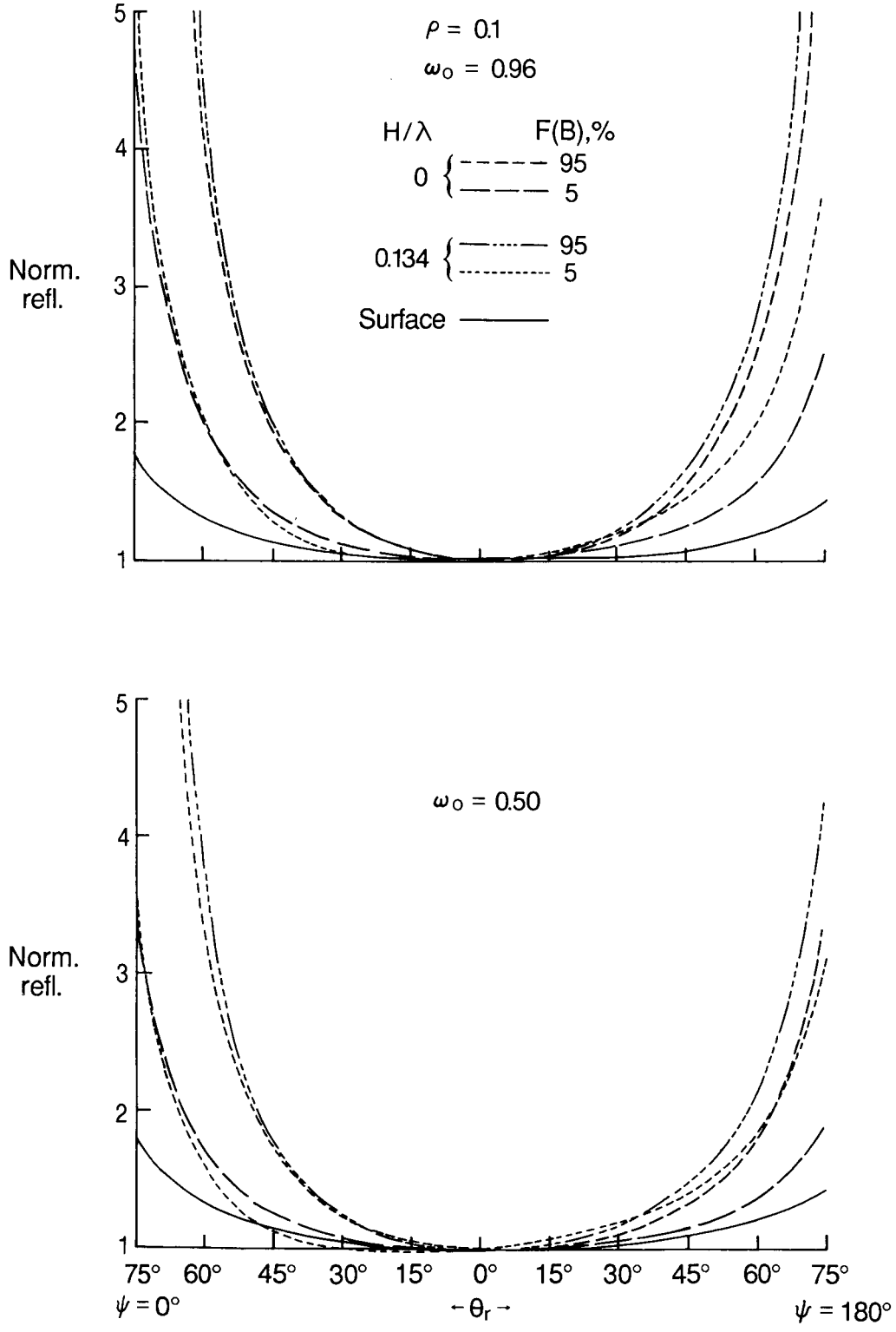

Figure 12. Normalized reflectances in the principal plane for $\rho = 0.1$, $\theta_s = 75°$, and $\omega_o = 0.96$ and 0.50. The surface reflectance is shown for comparison in figures 12 to 14.

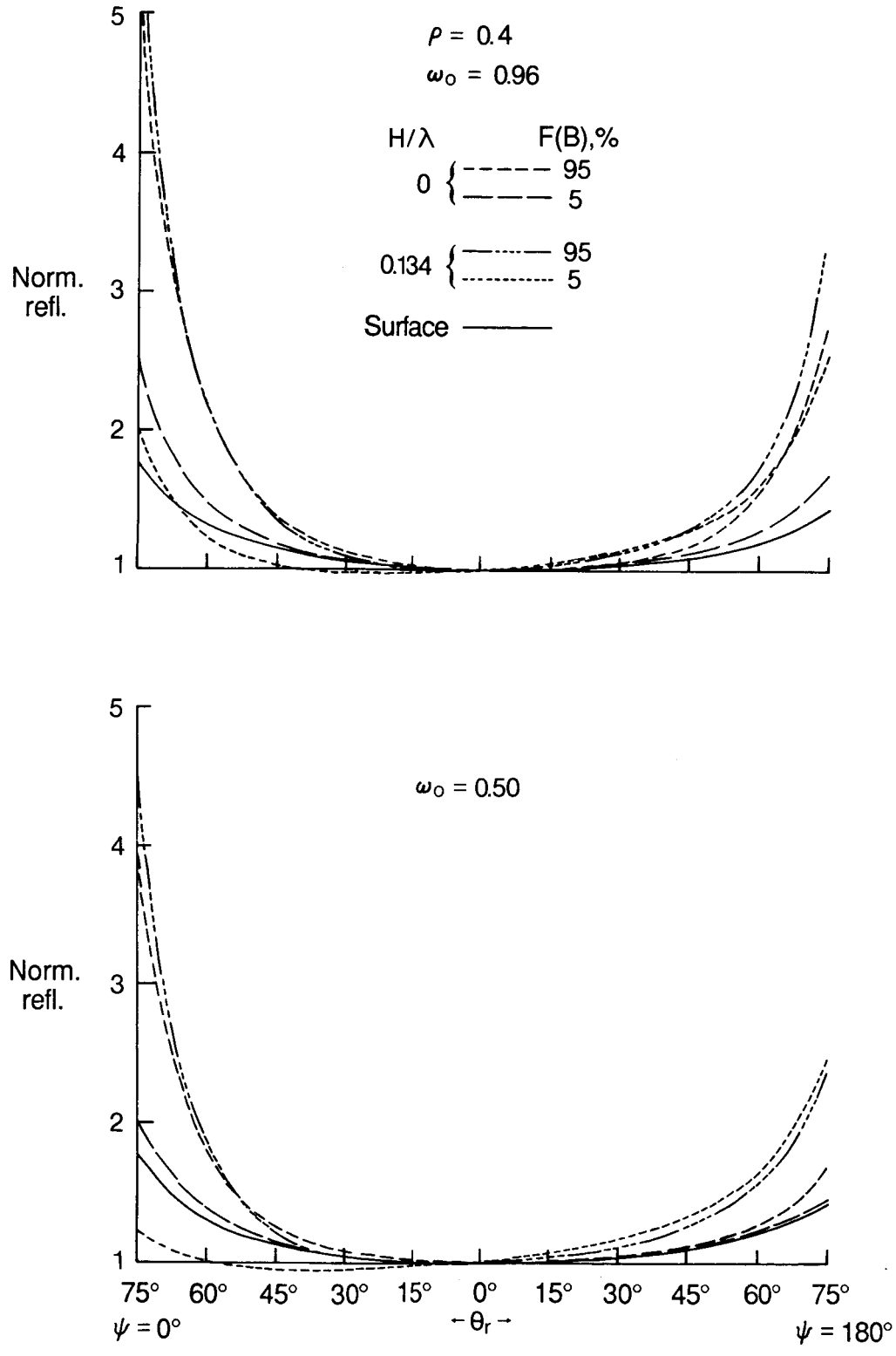

Figure 13. Normalized reflectances in the principal plane for $\rho = 0.4$, $\theta_s = 75°$, and $\omega_o = 0.96$ and 0.50.

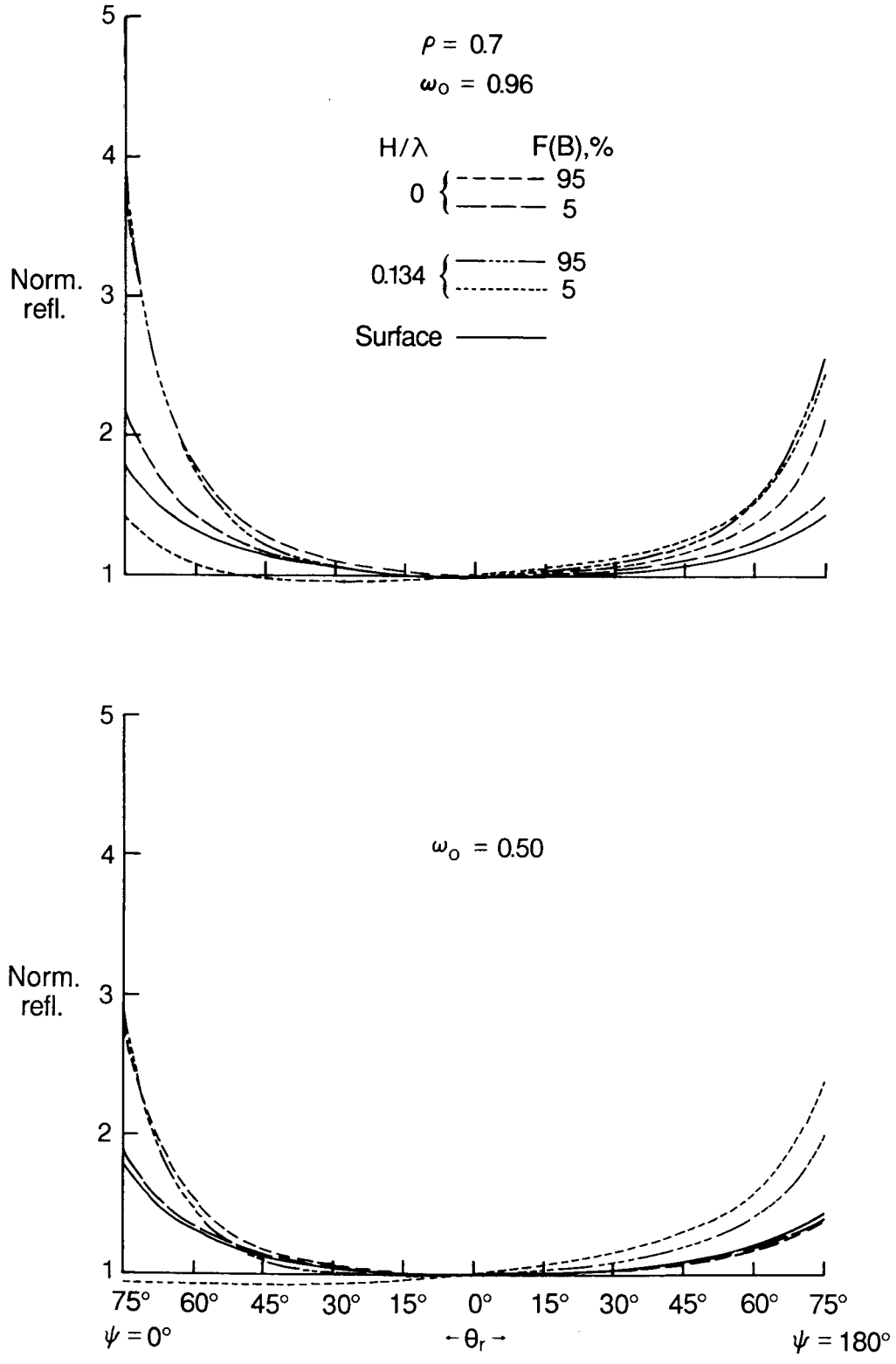

Figure 14. Normalized reflectances in the principal plane for $\rho = 0.7$, $\theta_s = 75°$, and $\omega_o = 0.96$ and 0.50.

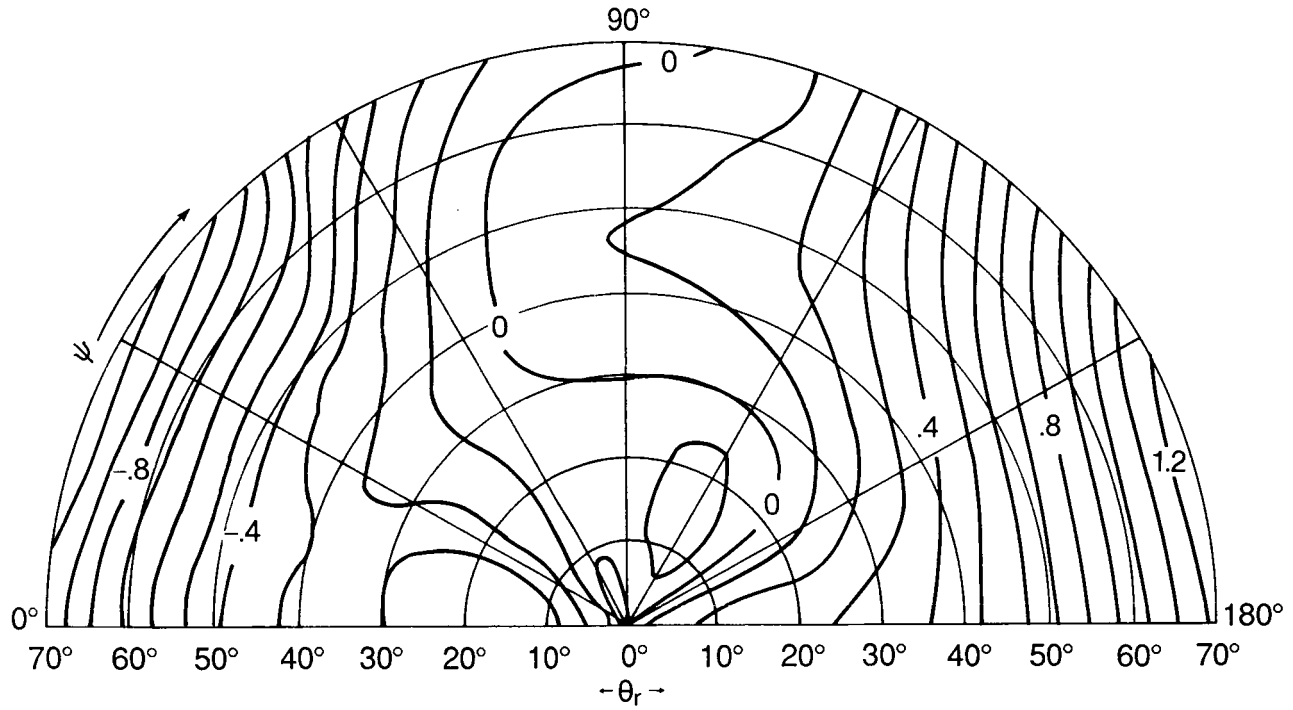

Figure 15. Plot of differences between the reflectance model of Salomonson in figure 2 and the flight results of Davis (1982). (Redrawn from Davis, 1982.) Positive values indicate that brighter features were measured by Davis.

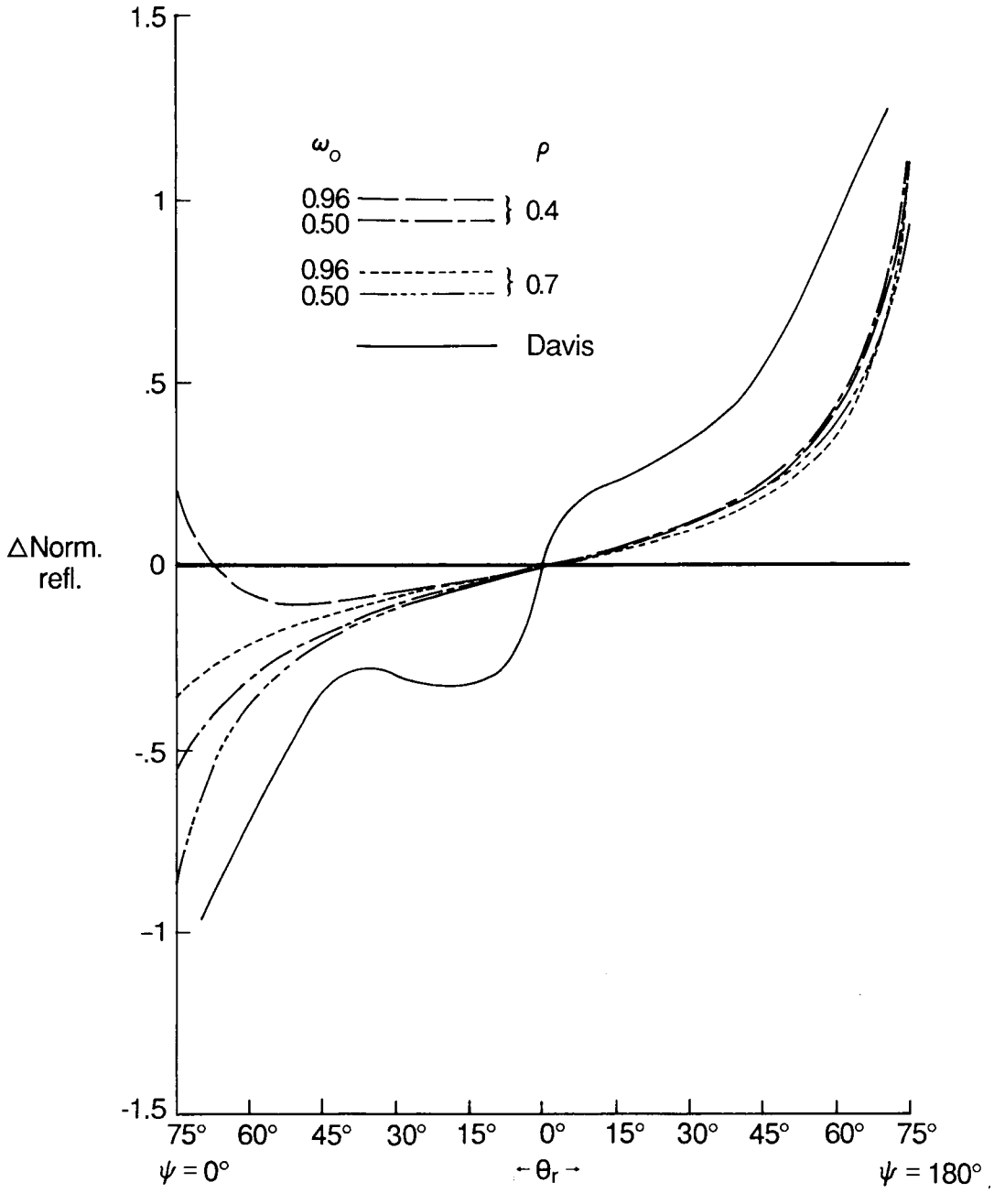

Figure 16. Effect of variations in ω_o and ρ for $\theta_s = 75°$, $F(B) = 5$ percent, and $H/\lambda = 0.134$. A more positive number indicates a higher calculated reflectance in figures 16 to 19. The results from Davis are shown for comparison.

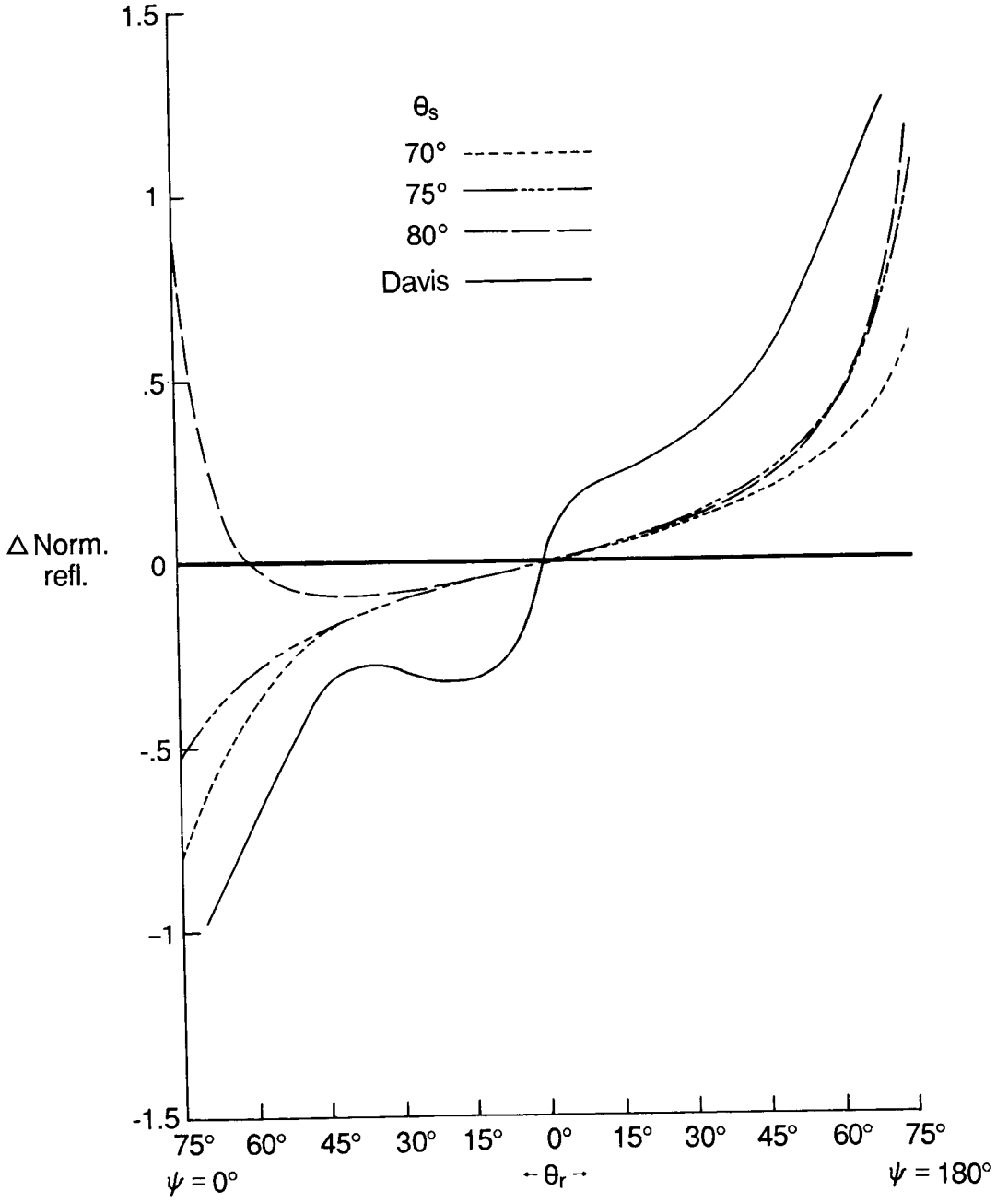

Figure 17. Effect of varying θ_s from 70° to 80° for $\rho = 0.4$, $\omega_o = 0.50$, $F(B) = 5$ percent, and $H/\lambda = 0.134$.

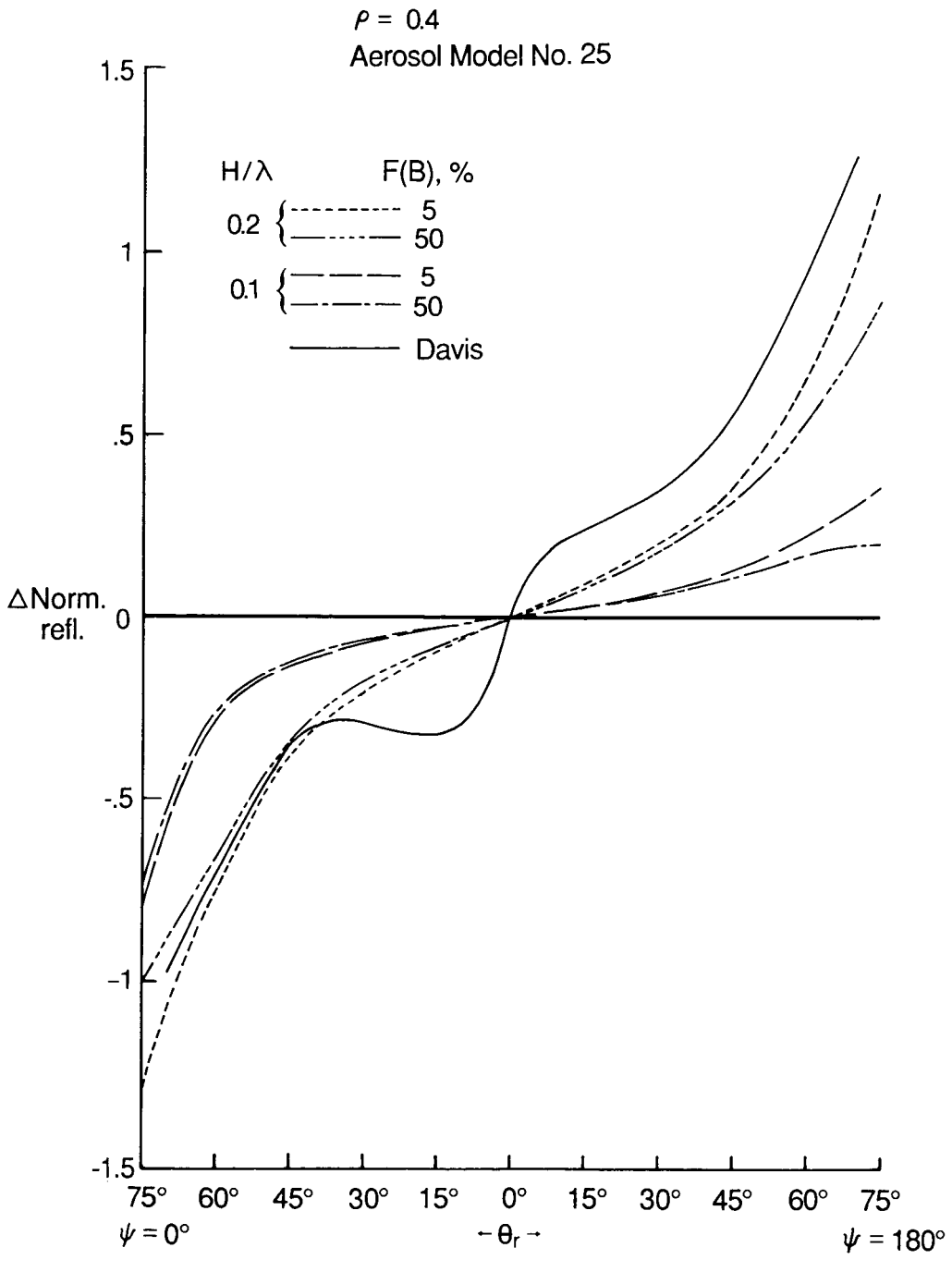

Figure 18. Effect of shadowing variations with aerosol model No. 25 and $F(B) = 5$ percent and 50 percent for $\rho = 0.4$, $\theta_s = 70°$, and $\omega_o = 0.50$.

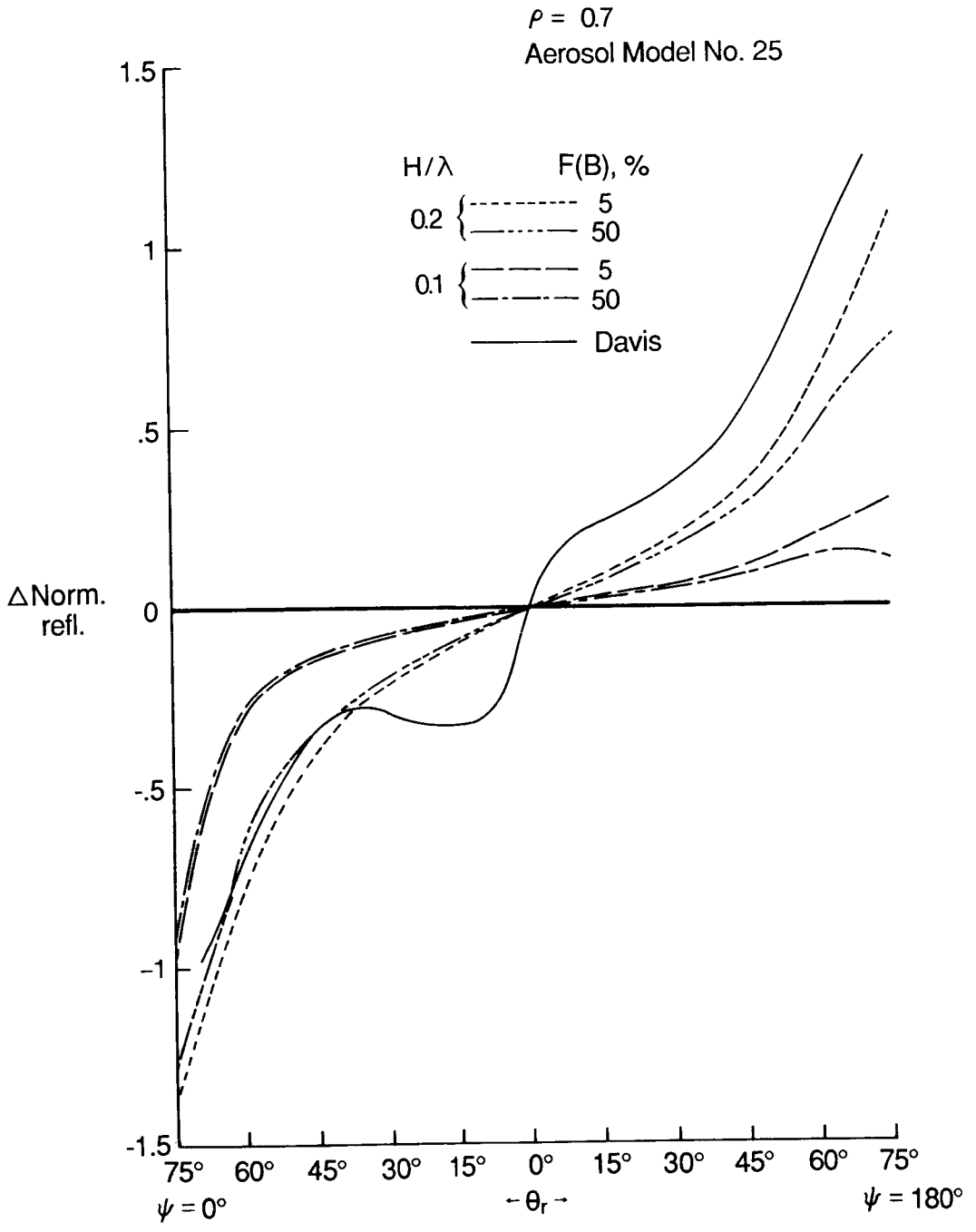

Figure 19. Effect of shadowing variations with aerosol model No. 25 and $F(B) = 5$ percent and 50 percent for $\rho = 0.7$, $\theta_s = 70°$, and $\omega_o = 0.50$.

NASA
National Aeronautics and Space Administration

Report Documentation Page

1. Report No.	2. Government Accession No.	3. Recipient's Catalog No.
NASA TP-2756		

4. Title and Subtitle	5. Report Date
Effects of Aerosols and Surface Shadowing on Bidirectional Reflectance Measurements of Deserts	September 1987
	6. Performing Organization Code
7. Author(s)	8. Performing Organization Report No.
David E. Bowker and Richard E. Davis	L-16327
9. Performing Organization Name and Address	10. Work Unit No.
NASA Langley Research Center Hampton, VA 23665-5225	549-01-31
	11. Contract or Grant No.
12. Sponsoring Agency Name and Address	13. Type of Report and Period Covered
National Aeronautics and Space Administration Washington, DC 20546-0001	Technical Paper
	14. Sponsoring Agency Code

15. Supplementary Notes

16. Abstract

Desert surfaces are probably one of the most stable of the Earth's natural targets for remote sensing. The bidirectional reflectance properties of one of these deserts, the Saudi Arabian desert, was investigated by J. M. Davis (NASA CP-2239, pp. 45–51) during the Summer Monsoon Experiment (Summer Monex). A comparison by Davis of his high-altitude measurements with near-surface measurements of the White Sands desert by Salomonson (Ph.D. Thesis, Colorado State Univ.) showed significant differences. Davis attributed these discrepancies to forward scattering of the dust-laden atmosphere prevalent during Summer Monex. The present paper is concerned in general with modeling the effects of atmospheric aerosols and surface shadowing on the remote sensing of bidirectional reflectance factors of desert targets, and in particular with comparing the results of these models with the flight results of Davis. Although it is possible to approximate Davis' results in this way, it is felt that a surface reflectance model with a smaller specular component would have permitted using a more realistic set of atmospheric conditions in the simulations.

17. Key Words (Suggested by Authors(s))	18. Distribution Statement
Bidirectional reflectance Aerosols Shadowing effects Atmospheric modeling Reflectance measurements Desert reflectances Desert atmospheres	Unclassified—Unlimited Subject Category 43

19. Security Classif.(of this report)	20. Security Classif.(of this page)	21. No. of Pages	22. Price
Unclassified	Unclassified	24	A02

NASA FORM 1626 OCT 86

NASA-Langley, 1987

For sale by the National Technical Information Service, Springfield, Virginia 22161-2171